1521-009X/50/9/1259–1271$35.00
DRUG METABOLISM AND DISPOSITION

dx.doi.org/10.1124/dmd.122.000884
Drug Metab Dispos 50:1259–1271, September 2022

Defining the Selectivity of Chemical Inhibitors Used for Cytochrome P450 Reaction Phenotyping: Overcoming Selectivity Limitations with a Six-Parameter Inhibition Curve-Fitting Approach[S]

Angela C. Doran, Woodrow Burchett, Connor Landers, Gabrielle M. Gualtieri, Amanda Balesano, Heather Eng, Alyssa L. Dantonio, Theunis C. Goosen, and R. Scott Obach

Department of ADME Sciences in Medicine Design, Pfizer Worldwide Research, Development & Medical, Groton, Connecticut (A.C.D., C.L., G.M.G., A.B., H.E., A.L.D., T.C.G., R.S.O.) and Department of Nonclinical Statistics in Early Clinical Development, Pfizer Worldwide Research, Development & Medical, Groton, Connecticut (W.B.)

Received March 2, 2022; accepted June 9, 2022

ABSTRACT

The utility of chemical inhibitors in cytochrome P450 (CYP) reaction phenotyping is highly dependent on their selectivity and potency for their target CYP isoforms. In the present study, 17 inhibitors of CYP1A2, 2B6, 2C8, 2C9, 2C19, 2D6, and 3A4/5 commonly used in reaction phenotyping were evaluated for their cross-enzyme selectivity in pooled human liver microsomes. The data were evaluated using a statistical desirability analysis to identify (1) inhibitors of superior selectivity for reaction phenotyping and (2) optimal concentrations for each. Among the inhibitors evaluated, α-naphthoflavone, furafylline, sulfaphenazole, tienilic acid, *N*-benzylnirvanol, and quinidine were most selective, such that their respective target enzymes were inhibited by ~95% without inhibiting any other CYP enzyme by more than 10%. Other commonly employed inhibitors, such as ketoconazole and montelukast, among others, were of insufficient selectivity to yield a concentration that could adequately inhibit their target enzymes without affecting other CYP enzymes. To overcome these shortcomings, an experimental design was developed wherein dose response data from a densely sampled multi-concentration inhibition curve are analyzed by a six-parameter inhibition curve function, allowing accounting of the inhibition of off-target CYP isoforms inhibition and more reliable determination of maximum targeted enzyme inhibition. The approach was exemplified using rosiglitazone *N*-demethylation, catalyzed by both CYP2C8 and 3A4, and was able to discern the off-target inhibition by ketoconazole and montelukast from the inhibition of the targeted enzyme. This methodology yields more accurate estimates of CYP contributions in reaction phenotyping.

SIGNIFICANCE STATEMENT

Isoform-selective chemical inhibitors are important tools for identifying and quantifying enzyme contributions as part of a cytochrome P450 (CYP) reaction phenotyping assessment for projecting drug-drug interactions. However, currently employed practices fail to adequately compensate for shortcomings in inhibitor selectivity and the resulting confounding impact on estimates of the CYP enzyme contribution to drug clearance. In this report, we describe a detailed half maximal inhibitory concentration (IC_{50}) study design with 6-parameter modeling approach that yields more accurate estimates of enzyme contribution.

Introduction

Interpatient variability in drug exposure is an important reason underlying variable drug response. Exposure is a function of the drug clearance rate and, if administered orally, the extent of drug absorption. Mechanisms of drug clearance include direct excretion and/or metabolism, with the latter being most prevalent. Among drug metabolizing enzymes, the cytochrome P450 (CYP) family is most frequently involved in metabolic drug clearance (Cerny, 2016). Activities of individual CYP enzymes can vary among individuals due to pharmacogenetic differences, drug interactions, and disease state, as well as other intrinsic and environmental factors. Thus, identification of specific CYP enzymes involved in metabolism and their respective quantitative contributions can offer great insight into interpatient variability in drug exposure and, hence, pharmacological response. The in vitro experiments conducted to quantitatively identify individual CYP enzymes in the metabolism of drugs have been termed "CYP reaction phenotyping" (Rodrigues, 1999; Zhang et al., 2007; Lu et al., 2003; Zientek et al., 2015). The data generated from these experiments comprise an important part of drug development required for understanding interpatient variability in exposure and drug-drug interactions.

CYP reaction phenotyping is conducted using the following experiment types, with intention of general agreement between two orthogonal methods employed: (Bjornsson et al., 2003; Bohnert et al., 2016; US FDA, 2020; EMA, 2012): (1) effect of CYP selective inhibitors or inhibitory antibodies on drug metabolism in a human-derived hepatic in vitro system; (2) measurement of the drug metabolism rates in individual CYP enzymes and scaling to reflect the whole liver; (3) comparison of drug

This work received no external funding.
No author has an actual or perceived conflict of interest with the contents of this article.
dx.doi.org/10.1124/dmd.122.000884.
[S] This article has supplemental material available at dmd.aspetjournals.org.

ABBREVIATIONS: CYP, cytochrome P450; f_m, fraction metabolized; $f_{u,\ mic}$, microsomal unbound fraction; HLM, human liver microsome; IC_{50}, half-maximal inhibitory concentration; $IC_{50,u}$, unbound half-maximal inhibitory concentration; IC_{95}, concentration of 95% inhibition; LC-MS/MS, liquid chromatography with tandem mass spectrometer; MAX, maximal percent inhibition; MRM, multiple reaction monitoring; PPP, 2-phenyl-2-1(1-piperidinyl)propane; Q1, first quadrupole of triple quadrupole mass spectrophotometer; Q3, third quadrupole of triple quadrupole mass spectrophotometer; TDI, time-dependent inhibitor.

metabolism rates to those of a set of CYP selective substrates across a panel of individual liver microsomes with specific polymorphic CYP enzyme expression (e.g., "correlation analysis"). While these methods have been employed for well over 20 years, they each suffer from some shortcomings. (1) Substrates and chemical inhibitors have imperfect selectivity for their intended CYP enzymes (Nirogi et al., 2015; Khojasteh et al., 2011; Lu et al., 2003). (2) Inhibitory antibodies fail to yield maximal inhibition (Shou et al., 2000; Polsky-Fisher et al., 2006). (3) Scaling factors needed for rate data obtained from individual enzymes can vary with the marker substrates used in their derivation (Dantonio et al., 2022; Lindmark et al., 2018; Wang et al., 2019; Siu and Lai, 2017). (4) Correlation analysis is not a quantitative method and generally requires one dominant CYP enzyme to observe a strong correlation (Ogilvie et al., 2008; Wienkers et al., 2002). (5) Genotyped reagents prepared from individuals may not reflect a global average population. (6) CYP reaction phenotyping is further confounded when the drug is metabolized slowly, requiring the measurement of metabolite as opposed to the simpler approach of measuring substrate consumption.

In our own laboratories, when using a panel of chemical inhibitors to quantitatively identify CYP enzymes involved in the metabolism of a new drug candidate, we frequently observe the sum of inhibition across the chemical inhibition panel exceeding 100%. This outcome confounds subsequent fraction metabolized (f_m) calculations by overestimating minor isoforms (due to non-selectivity) and diluting contribution of major isoforms (when normalized to 100%), thereby skewing the isoform profile when the underlying limitations of inhibitor selectivity are not considered. If using standard binding theory, the inhibitor selectivity must be 1000-fold to yield 99% inhibition of a target CYP and not cause more than 10% inhibition of off-target CYPs. The inhibitors commonly employed for CYP reaction phenotyping do not possess this degree of selectivity, and the resulting spillover inhibition when using single concentrations leads to incorrect assignment of minor contributing isoforms. Furthermore, even for the most widely employed CYP inhibitors, there is a wide range of reported potency values (Fig. 1), and these can be confounded by experimental conditions, such as variance in non-specific binding with microsomal concentration and marker substrate concentration used relative to its Michaelis-Menten parameter.

To address this issue, 17 CYP-selective inhibitors were thoroughly characterized for quantitation of on- and off-target selectivity. Additionally, a multiple-concentration inhibitor study design employing a six-parameter curve-fitting approach is proposed to exclude off-target effects and lead to improved quantitation of f_m. The application of combined inhibitor selectivity knowledge with a data-rich 22-point concentration experimental design is exemplified using rosiglitazone *N*-demethylation activity for estimation of CYP3A and CYP2C8 f_m. A comparison of single- and multiple-concentration approaches highlights the pitfalls of previous practices. Adoption of this methodology and incorporation into a broader integrated, sequential two-step approach, as described in the accompanying report in this journal (Dantonio et al., 2022), should offer substantial improvement to the current CYP reaction phenotyping practices.

Materials and Methods

Materials. Experiments were conducted on human tissue acquired from a vendor that was verified as compliant with internal policies, including institutional review board/independent ethics committee approval. Pooled human liver microsomes of low CYP3A5 expression, prepared from 50 mixed-sex donors, were purchased from Sekisui XenoTech (Kansas City, KS). cDNA expressed human CYP3A4 Supersomes and untransfected baculosome control were purchased from Corning (Corning, NY).

Chemicals and solvents of high-performance liquid chromatography or analytical grade were purchased from Fisher Scientific (Waltham, MA). Monobasic and dibasic potassium phosphate buffers, $MgCl_2$, NADPH, and DMSO were purchased from Sigma-Aldrich (St. Louis, MO). Substrates were purchased from either Sigma-Aldrich (St. Louis, MO), US Pharmacopeia (Rockville, MD), or Toronto Research Chemicals (North York, Ontario, Canada), except for rosiglitazone, which was synthesized internally at Pfizer (Groton, CT). The 17 chemical inhibitors tested (typical purity >95%) were either synthesized internally at Pfizer, Groton, CT or purchased from one of the following sources: Sigma-Aldrich (St. Louis, MO) (ex. CYP3cide), Toronto Research Chemicals (Ontario, Canada), MedChemExpress (Monmouth Junction, NJ), US Pharmacopeia (Rockville, MD), or Enzo Life Sciences (Ann Arbor, MI). Deuterated analytes used as internal standards were synthesized internally at Pfizer (Groton, CT).

The equilibrium dialysis apparatus and Spectra Por (MWCO 12–14K) cellulose dialysis membranes for microsomal binding experiments were obtained from Repligen (formerly Spectrum, Boston, MA).

Inhibitor Selectivity in CYP2B6 and CYP-Selective Probe Cocktail Assays. The effects of selective chemical inhibitors on the CYP-mediated metabolism of probe substrates were characterized using pooled HLM under verified conditions of linear product formation. Incubations (200 µl) were conducted in 100 mM of potassium phosphate buffer (pH 7.4) containing 3.3 mM of $MgCl_2$, 1.2 mM of NADPH, 0.03 mg/ml microsomal protein, and probe substrates at 37°C in a heat block. A series of 100X concentrated inhibitor stock solutions were prepared by serial dilution for testing across a broad concentration range. For incubations containing competitive inhibitors, microsomes were prewarmed with inhibitors for 5 minutes prior to initiating the reactions by the sequential addition of NADPH followed immediately by substrate (see below). Incubations containing time dependent inhibitors (TDI) were preincubated with HLM, the inactivator, and NADPH for 10 minutes to achieve complete inactivation of the respective CYP isoform. Reactions were initiated by the addition of 10X concentrated substrate stock solution containing a cocktail of the CYP-specific probe substrates, phenacetin (6 µM, CYP1A2), amodiaquine (0.33 µM, CYP2C8), diclofenac (1.3 µM, CYP2C9), mephenytoin (7.9 µM, CYP2C19), dextromethorphan (0.36 µM, CYP2D6), and midazolam (0.42 µM, CYP3A4), prepared in a mixture of aqueous and organic solvents (acetonitrile or methanol) to achieve final incubation concentrations of approximately 1/5 Michaelis-Menten parameter based on in-house determined kinetics (Supplemental Table 1) (Walsky and Obach, 2004). The final solvent concentration in the incubation was <1%. Reactions were terminated after 14 minutes by quenching 125-µl aliquots of incubation mixture into 200 µl of acetonitrile containing internal standard. Following vortex mixing and centrifugation at 1700 x *g* for 5 minutes, the resulting supernatants (225 µl) were transferred to clean 96-well plates, concentrated under a stream of warm nitrogen, and reconstituted in 100 µl of 90/10 water/acetonitrile for compatibility with initial liquid chromatography with tandem mass spectrometer (LC-MS/MS) conditions.

Separate incubations for the assessment of CYP2B6 activity were conducted in a similar fashion as described above with the following modifications: the substrate stock solutions contained bupropion (18 µM) alone, reactions were terminated after 20 minutes by quenching of 100-µl aliquots with 200 µl of acetonitrile containing internal standard. All HLM selective chemical inhibition incubations were conducted in duplicate. Detailed study conditions are described in the Supplemental Table 1.

Ketoconazole and Montelukast Inhibition of Rosiglitazone Metabolism in HLM. Using similar incubation conditions described for the cocktail substrate assay above, reactions (400 µl) with 0.1 mg/ml of HLM protein and inhibitors were initiated by addition of the substrate rosiglitazone (1 µM) and quenched at 30 minutes by protein precipitation with acetonitrile containing internal standard. Incubations were conducted in triplicate.

LC-MS/MS Methodology for Quantitation of Probe Substrates and Rosiglitazone. All microsomal incubation samples were quantitated by LC-MS/MS bioanalysis conducted using a Sciex Triple Quad 6500 mass spectrometer (Framingham, MA) with an electrospray ion source, Agilent 1290 binary pump (Santa Clara, CA), and CTC Analytics autoinjector (Zwingen, Switzerland).

Cocktail Assay. The aqueous mobile phase (A) was comprised of 0.1% acetic acid in water, and the organic mobile phase (B) consisted of acetonitrile. Samples (10 µl) from the in vitro incubations were injected onto an Acquity BEH C18 (2.5 × 50 mm, 1.7 µm) (Waters, Milford, MA) column at room temperature with a flow rate of 0.5 ml/min. The gradient program began with 2% initial mobile phase B with a linear gradient to 45% B over 2.2 minutes, then to 90% over 0.2 minutes, held at 90% B for 0.5 minutes, and followed by re-equilibration to initial conditions for 0.6 minutes. The mass spectrometer was operated in multiple reaction

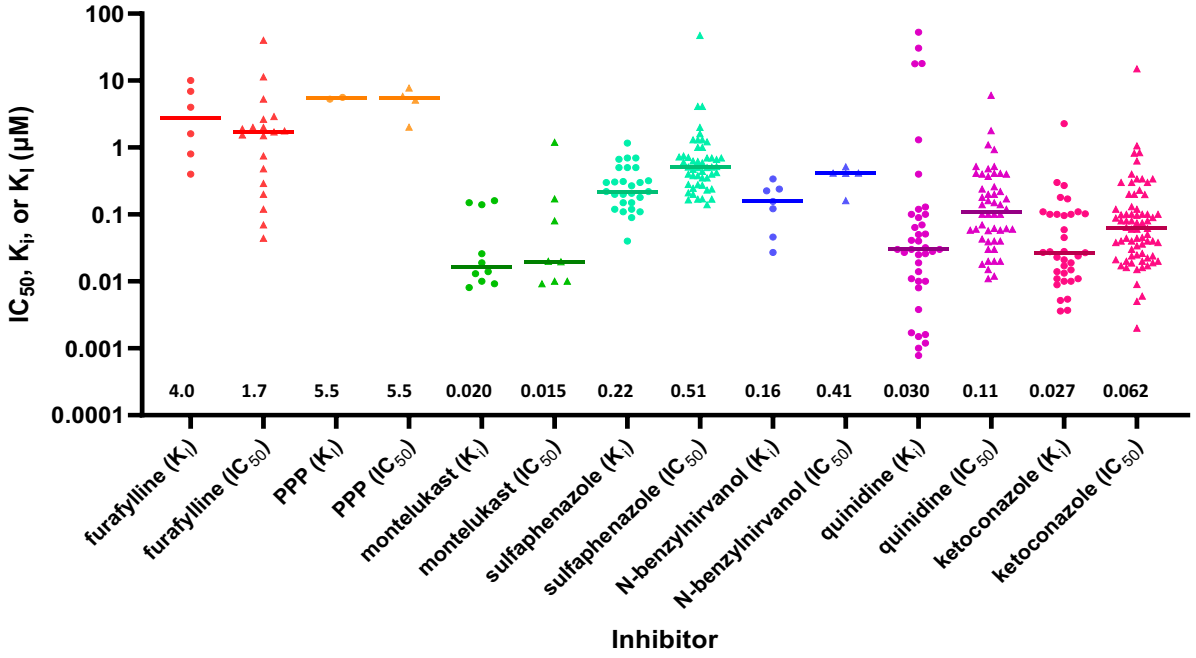

Fig. 1. Summary of Potency Values Reported in the Scientific Literature for Common Cytochrome P450 Inhibitors. Data were obtained from the University of Washington Drug Interaction Database (https://www.druginteractionsolutions.org/). IC_{50}, K_i, and K_I values were restricted to those measured in human liver microsomes and recombinant P450 enzymes. Reactions were restricted to phenacetin *O*-deethylase and tacrine 1'-hydroxylase, bupropion hydroxylase, amodiaquine *N*-deethylase and paclitaxel 6α-hydroxylase, diclofenac 4'-hydroxylase, (S)-warfarin 7-hydroxylase, and tolbutamide 4-hydroxylase, (S)-mephenytoin 4'-hydroxylase and omeprazole 5-hydroxylase, bufuralol 1'-hydroxylase and dextromethorphan *O*-demethylase, and midazolam 1'-hydroxylase and testosterone 6β-hydroxylase. Horizontal bars and displayed numeric values represent the median values.

monitoring mode (MRM) while monitoring positive ion detection with the following mass transitions (first quadrupole of triple quadrupole mass spectrophotometer [Q1]/third quadrupole of triple quadrupole mass spectrophotometer [Q3]) and collision energies (in parenthesis): 4'-hydroxymephenytoin 235/150 (26), [$^2H_3$]-4'-hydroxymephenytoin 238/150 (26), N-desmethylamodiaquine 328/283 (23), [$^2H_5$]-N-desmethylamodiaquine 333/283 (23), dextrorphan 258/201 (31), [$^2H_3$]-dextrorphan 261/201 (34), 1'-hydroxymidazolam 342/324 (30), [$^2H_4$]-1'-hydroxymidazolam 346/328 (30), acetaminophen 152/110 (22), [$^2H_7$]-acetaminophen 159/115 (22), hydroxydiclofenac 312/230 (29), and [$^{13}C_6$]-hydroxydiclofenac 318/236 (20). It is noted that during bioanalytical development, the removal of formic acid from all samples and mobile phases was necessary to eliminate background interferences in the 4'-hydroxymephenytoin MRM channel and monthly replacement of Mobile Phase A was required to maintain overall chromatographic performance. Additionally, extra effort was taken to ensure chromatographic separation of acetaminophen from a peak arising from in-source fragmentation of phenacetin.

CYP2B6 Assay. Chromatographic separation of the CYP2B6 incubation samples was achieved following injection (10 µl) onto a Halo C18 (2.1 × 10 mm, 2.7 µm) (Advanced Materials Technology, Wilmington, DE) column at room temperature with a flow rate of 0.5 ml/min. The aqueous mobile phase (A) was comprised of 0.1% formic in water and organic mobile phase (B) consisted of 0.1% formic acid in acetonitrile. The gradient program began with 5% initial mobile phase B with a linear gradient to 95% B over 0.9 minutes, held at 95% B for 0.3 minutes, and followed by re-equilibration to initial conditions for 0.6 minutes. The mass spectrometer was operated in MRM mode while monitoring positive ion detection and collision energy 36, following mass transitions (Q1/Q3) for hydroxybupropion 256/130, and [$^2H_6$]-hydroxybupropion 262/130.

Rosiglitazone Assay. Chromatographic analysis of *N*-desmethylrosiglitazone and internal standard was achieved using aqueous mobile phase (A) comprised of 0.1% formic in water and organic mobile phase (B) consisting of 0.1% formic acid in acetonitrile. Samples (10 µl) from the in vitro incubations were injected onto an Acquity BEH C18 (2.1 × 50 mm, 1.7 µm) (Waters, Milford, MA) column at room temperature with a flow rate of 0.5 ml/min. The gradient program began with 2% initial mobile phase B for 0.5 minute with a linear gradient to 35% B over 1.1 minutes, stepped immediately to 95% B after 0.01 minutes, held at 95% B for 0.3 minutes, and followed by re-equilibration to initial conditions for 0.6 minutes. The mass spectrometer was operated in MRM mode, while monitoring positive ion detection and collision energy (35), with the following mass transitions (Q1/Q3) for rosiglitazone 358/135, N-desmethylrosiglitazone 344/121, and [$^2H_4$]-N-desmethylrosiglitazone 348/125.

Microsomal Binding of CYP-Selective Chemical Inhibitors. Human liver microsomes were diluted to 0.03 or 0.1 mg/ml of protein in 100 mM of potassium phosphate buffer (pH 7.45) and spiked with 1000X concentrated inhibitor stock solution, prepared in DMSO, to achieve a final drug concentration of 1.0 µM. Aliquots (1 ml) of the prepared microsome solution were prewarmed to 37°C and loaded into one side of a Spectrum equilibrium dialysis cell prepared with a SpectraPor (Repligen, Boston, MA) 12-14 kDA cellulose membrane, prepared per manufacturer's instructions. The microsomes were dialyzed against an equal volume of 100 mM of potassium phosphate buffer of pH 7.45. The entire apparatus was incubated for 18 hours under constant rotation while submerged in a 37°C water bath. Samples were processed using a mixed-matrix protein precipitation method and analyzed by LC-MS/MS. To each sample, an equal volume of opposing control buffer or microsome solution was added resulting in common matrix composition across all donor and receiver samples. Aliquots (0.6 ml) of the mixed matrix samples were precipitated with a 5X volume of acetonitrile and 0.1 ml of internal standard (1 µM of clozapine), vortexed, then centrifuged at 1800 x *g* for 5 minutes. The supernatants were evaporated to dryness under vacuum centrifuge and residues reconstituted in 0.1 ml of 20/80 acetonitrile/water containing 1% formic acid, for analysis by LC-MS/MS.

The LC-MS/MS system used for quantitation of nonspecific binding samples consisted of an Orbitrap Elite mass spectrometer with ion spray source, Accela Quanternary UHPLC pump (Thermo-Fisher; Waltham, MA), and CTC Analytics autoinjector. Aqueous mobile phase (A) was comprised of 0.1% formic acid in water and organic mobile phase (B) consisted of acetonitrile. Samples (10 µl) were injected onto a Phenomenex Kinetex C_{18} (2.1 × 50 mm, 1.7 µm) (Phenomenex, Torrance, CA) column at room temperature with a flow rate of 0.4 mL/min. The gradient program began with 2% initial mobile phase B with a linear gradient to 15% B over 3.5 minutes, then to 50% over 3 minutes, to 80% over 0.9 minutes, held at 95% B for 0.5 minutes, and followed by re-equilibration to initial conditions for 1 minute. Slight modifications to the bioanalytical method for analysis of gemfibrozil glucuronide binding samples included aqueous mobile phase A comprised of 10 mM of ammonium acetate, organic mobile phase B consisting of

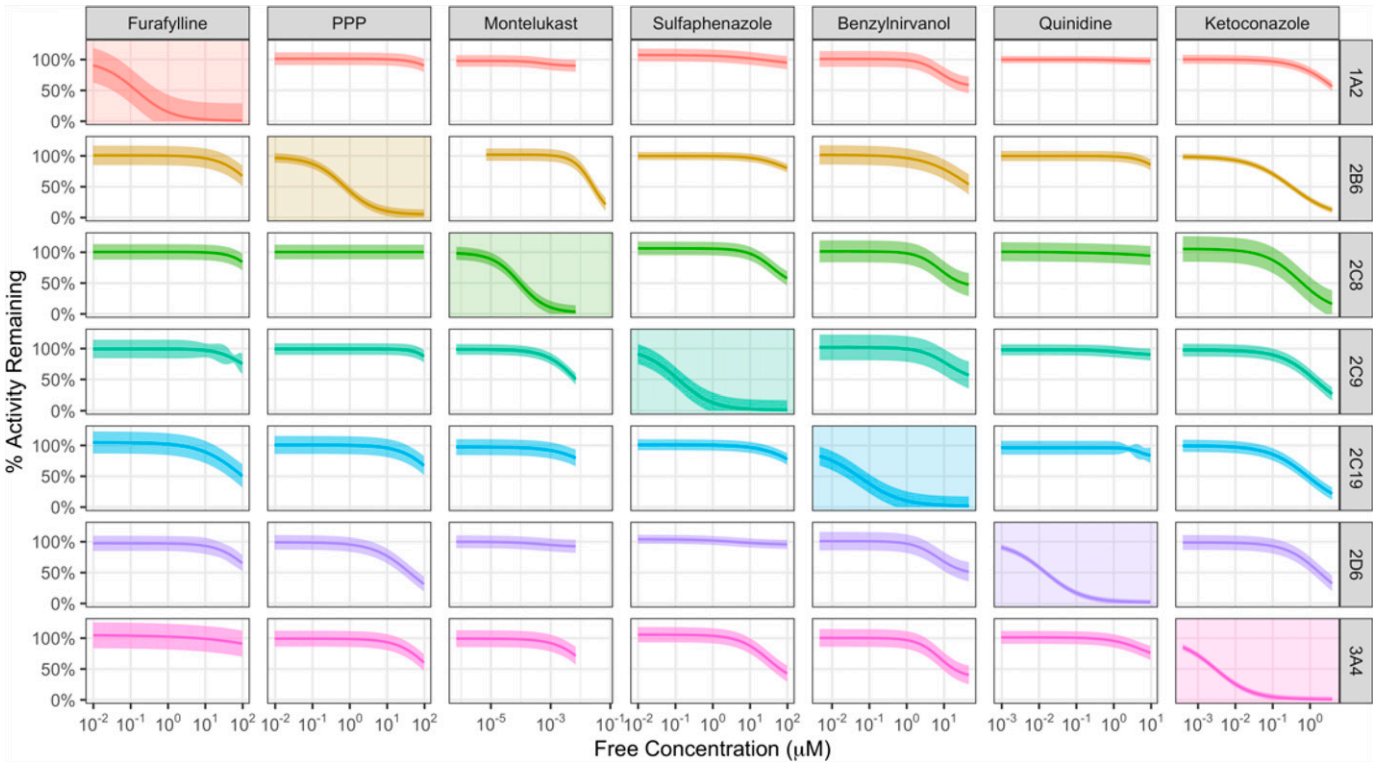

Fig. 2. Inhibition Curves for Commonly Used Inhibitors. Data represent line of best fit (solid line) and 95% confidence interval (shaded) from $N = 2$–3 experiments. Abbreviations: PPP, 2-phenyl-2-(1-piperidinyl)propane.

acetonitrile, and the gradient program beginning with 5% B, increased linearly to 95% B over 3.5 minutes, then held for 1 minute at 95% B, and re-equilibrated to initial conditions for 0.9 minutes.

The mass spectrometer was set to MS1 scan mode (m/z 100–900) at a resolution setting of 30,000 and operated in positive ion mode for all analytes except gemfibrozil glucuronide. Response for each analyte was determined by post-analysis construction of the extracted ion chromatograms of protonated molecular ion (deprotonated for gemfibrozil glucuronide) to a high-resolution mass accuracy of 5 ppm.

Due to challenges with nonspecific binding and/or chemical instability observed during equilibrium dialysis, the microsomal binding of troleandomycin was assessed by measuring inhibition of midazolam 1'-hydroxylase marker activity in incubations of spanning inactive protein concentrations while maintaining a consistent active protein concentration. The effect of troleandomycin nonspecific binding was assessed in incubations (150 μl) with recombinant human CYP3A4 (0.01 mg/ml) diluted in 100 mM potassium phosphate buffer pH 7.4 containing 3.3 mM of $MgCl_2$, 1.2 mM of NADPH, and 0.43 μM of midazolam. Manipulation of the background protein concentration was achieved by supplementation with untransfected baculosome, resulting in a range of protein concentrations from 0.01 to 3 mg/ml. Troleandomcyin was prepared as a series of 100X concentrated stock solutions in 50/50 methanol/water, to enable testing across a range of inhibitor concentrations for IC_{50} determination. Reactions were initiated by addition of NADPH and incubated for 4 minutes at 37°C in a heat block.

Microsomal samples for determination of troleandomycin nonspecific binding were analyzed by LC MS/MS analysis. Chromatographic separation was achieved following injection (10 μl) onto a Halo C18 (2.1 × 30 mm, 2.7 μm) column at room temperature with a flow rate of 0.6 ml/min. The aqueous mobile phase (A) was comprised of 0.1% formic acid in water and organic mobile phase (B) consisted of 0.1% formic acid in acetonitrile. The gradient program began with 10% initial mobile phase B with a linear gradient to 90% B over 0.5 minutes, held at 90% B for 0.5 minutes, followed by re-equilibration to initial conditions for 0.55 minutes. The mass spectrometer operated in MRM mode while monitoring positive ion detection and collision energy 30, with the following mass transitions (Q1/Q3) for 1'-hydroxymidazolam of 342/324 and [$^2H_4$]-1'-hydroxymidazolam, 346/328.

Data Analysis

Inhibitor selectivity. The inhibitory profiles of each inhibitor were generated from the combined activity of 2–3 experiments using GraphPad Prism for Windows (version 9). The dose-response data were modeled by nonlinear regression using the 4-parameter logistic equation (referred to as the "4-parameter fit"):

$$Y = Bottom + \frac{Top - Bottom}{1 + e^{h(\ln x - \ln IC_{50})}} \quad (1)$$

where Y is the percent of control activity remaining and x is the inhibitor concentration. The four parameters in the model are the IC_{50}, which represents the inhibitor concentration that yields a response halfway between the upper and lower asymptotes, the hill slope (h), which represents the steepness of the curve, and the upper and lower asymptotes (*Top* and *Bottom*, respectively), which represent the maximum and minimum possible responses. The maximal contribution of a CYP was determined by the "span" or the difference between the fitted upper and lower asymptotes. Absolute IC_{50} values were reported whenever an inhibition of 50% or greater was observed within the inhibitor concentration range tested. The bottom asymptote was constrained to values greater than zero. Curve fitting parameters were denoted by subscripted letter u when adjusted for nonspecific microsomal binding (i.e., unbound inhibitor concentration).

Desirability Scoring. Optimal single inhibitor concentrations were determined using a desirability scoring approach (Derringer and Suich, 1980). Desirability functions map each endpoint (% activity remaining for on- and off-target CYPs, in this case) to a number between zero and one. These individual desirability scores were combined using a geometric mean to create a single desirability score for each concentration of an inhibitor. For target CYPs, lower % activity remaining was preferred, while higher % activity remaining was preferred for off-target CYPs (Supplemental Fig. 1). Specifically, the desirability score for the most inhibited off-target CYP started decreasing linearly from a score of 1 at 95% activity remaining to a score of 0 at 50% activity remaining. This was balanced with the desirability score for the target CYP, which started increasing linearly from a score of 0 at 50% relative activity remaining to a score of 1 at 0% relative activity remaining, where relative percent activity remaining refers to the percent activity remaining normalized to the upper and lower asymptote of the fitted 4-parameter logistic curve. This design minimizes the penalty to inhibitors that never fully inhibited the target enzyme, such as

α-naphthoflavone or CYP3cide. The overall desirability scores were used to rank the inhibitors, with more selective inhibitors having higher desirability scores.

Simulated Inhibition Profiles when Using 6-Parameter Model. The ability of a 6-parameter model to quantitate both target and off-target isoform contribution from a multiple concentration study design was investigated. Comparison of the theoretical concentration response profiles resulting from fitting to 6-parameter inhibition model (Fig. 4) was conducted under varying conditions of inhibitor potency, selectivity, and enzyme contribution,

$$Y = I_{max} - MAX_a + \left(\frac{MAX_A}{1 + e^{h(\ln x - \ln IC50A)}}\right) - MAX_b + \left(\frac{MAX_B}{1 + e^{\ln x - \ln IC50B}}\right) \quad (2)$$

where Y is the percent control activity remaining, and x is the inhibitor concentration. The six parameters in the model are MAX_A and MAX_B, which represent the maximum contribution of enzyme A and B, respectively, IC_{50A} and IC_{50B}, which are the inflection points for the inhibitor on enzymes A and B, respectively, the hill slope (h), which represents the steepness of the curve for enzyme A, and I_{max}, which represents the maximum possible response. The simulations were based on an inhibitor with a target potency of 0.001 μM IC_{50} and a second off-target IC_{50} of 10 μM, representing a selectivity of 10,000-fold. The effect of the inhibitor selectivity was modeled under assumptions of a single-enzyme contribution of 100%, or two enzymes contributing proportions of 60/40 or 70/30.

Rosiglitazone Dose Response Analysis. Data from test compounds (rosiglitazone) were fit using either a traditional 4-parameter dose-response curve (eq. 1) or a 6-parameter dose-response curve (eq. 2). Statistical comparison and model selection was conducted by analysis of an extra sum-of-squares F-test.

After fitting the dose-response curves to the test compound data, a two-one-sided t-tests (TOST) equivalence procedure was used to determine if the test compound IC_{50} was significantly within 5-fold of the probe substrate IC_{50} (Schuirmann, 1987; Walker and Nowacki, 2011). When the 6-parameter model was selected, the IC_{50} of the first phase (IC_{50A}) of the curve was compared with the IC_{50} from the probe substrate. If a significant 5-fold equivalence in IC_{50} values between the test compound and probe was established, the reduction in % activity of the test compound was compared with zero. For the 4-parameter model, the span parameter (difference between upper asymptote and lower asymptote) must be significantly greater than zero, while the MAX_A parameter must be significantly greater than zero for the 6-parameter model. If both the equivalence tests were passed and the decrease in activity was significantly greater than zero, then the inhibition of the target enzyme was deemed significant and reported.

Rosiglitazone Single Concentration Analysis. Statistical significance of inhibition at a single inhibitor concentration was determined using Welch's unpaired two-sample t-test with unequal variances (Welch, 1947) to compare the peak area ratios without any inhibitor to the peak area ratios with the inhibitor.

Results

Microsomal Binding. The extent of non-specific binding in vitro can be important for some CYP inhibitors requiring that inhibition potency values be corrected for this phenomenon. The fraction unbound (fu_{mic}) of 17 inhibitors were determined by equilibrium dialysis at 0.03 mg/ml of human liver microsomal protein, consistent with conditions used for measurement of CYP inhibition selectivity (*vide infra*). Values ranged from 0.00691 to unity (Table 1). Consistent with previous literature reports, montelukast exhibited the highest nonspecific binding among the inhibitors, with an fu_{mic} of 0.00691. Among the remaining inhibitors tested, dasotraline, ketoconazole, and α-naphthoflavone also demonstrated relevant nonspecific binding to microsomes with moderate fu_{mic} values of 0.218, 0.391, and 0.390, respectively. Nearly half (8 of 17) the inhibitors showed low affinity for microsomes as indicated by fu_{mic} values >0.9. Among these, only one inhibitor, troleandomycin, was characterized as having no nonspecific binding as indicated by fu_{mic} equivalent to 1 across all protein concentrations tested. Therefore, the nominal and unbound concentrations for this subset of select inhibitors were considered equivalent. For all other inhibitors, a correction for nonspecific binding during the incubations was applied during data analysis. Additional fu_{mic} values of 0.336 for ketoconazole and 0.00193 for montelukast were determined for a microsomal protein concentration of 0.1 mg/ml, the condition used during assessments of rosiglitazone metabolism (*vide infra*).

Inhibition Profiles. The selectivity profiles of 17 chemical inhibitors were determined against CYP-selective probe activity using a substrate cocktail assay in HLM for simultaneous characterization of inhibitory potency against the major human CYP isoforms CYP1A2, CYP2C8, CYP2C9, CYP2D6, and CYP3A4, as well as a separate assay of CYP2B6 activity. Inhibition plots are presented in Figs. 3 and 4 and absolute IC_{50} values, corrected for non-specific binding as appropriate, are reported in Table 2. Full inhibition parameters from curve fitting of cocktail and CYP2B6 inhibition are provided in Supplemental Table 2.

Inhibitors Targeting CYP1A2. α-Naphthoflavone was a highly potent inhibitor of CYP1A2 mediated phenacetin *O*-deethylase activity

TABLE 1

Nonspecific Binding of CYP-Selective Inhibitors to Microsomal Protein

Isoform	Inhibitor	Fraction Unbound at Varying Microsomal Protein Concentrations					
		0.01 mg/mL	0.03 mg/mL	0.1 mg/mL	0.3 mg/mL	1 mg/mL	3 mg/mL
CYP1A2	Furafylline	0.910 ± 0.189	0.980 ± 0.084	1.003 ± 0.067*	0.935 ± 0.111	0.903 ± 0.0738	0.890 ± 0.0378
	α-Napthoflavone	0.600 ± 0.0919	0.390 ± 0.0345	0.187 ± 0.0176	0.0912 ± 0.0135	0.0268 ± 0.00298	0.0109 ± 0.00258
CYP2B6	Dasotraline	0.407 ± 0.119	0.218 ± 0.0702	0.0639 ± 0.00504	0.0208 ± 0.00809	0.00809 ± 0.00148	0.00410 ± 0.000303
	PPP	0.925 ± 0.0557	0.967 ± 0.0349	0.999 ± 0.0240	0.918 ± 0.0681	0.875 ± 0.0389	0.787 ± 0.0248
	Ticlopidine	0.924 ± 0.0544	0.891 ± 0.0175	0.756 ± 0.0439	0.491 ± 0.0564	0.223 ± 0.0096	0.101 ± 0.0130
CYP2C8	Montelukast	0.057 ± 0.026	0.00691 ± 0.0015	0.00193 ± 0.0009	0.00101 ± 0.00040	0.000302 ± 0.00009	0.000170 ± 0.00001
	Gemfibrozil Glucuronide	0.761 ± 0.238	0.815 ± 0.022	0.872 ± 0.044	0.868 ± 0.134	0.977 ± 0.023	0.864 ± 0.052
CYP2C9	Sulfaphenazole	0.949 ± 0.118	0.985 ± 0.029	1.057 ± 0.0409*	1.034 ± 0.123*	0.949 ± 0.0880	0.764 ± 0.0307
	Tienilic Acid	1.041 ± 0.124*	0.980 ± 0.00647	0.938 ± 0.0350	0.914 ± 0.120	0.995 ± 0.0304	0.987 ± 0.0793
CYP2C19	N-Benzylnirvanol	0.965 ± 0.0874	0.925 ± 0.0341	0.911 ± 0.0135	0.822 ± 0.0635	0.758 ± 0.0317	0.490 ± 0.0621
	Esomeprazole	0.930 ± 0.0373	0.909 ± 0.00498	0.964 ± 0.0118	0.895 ± 0.0971	0.835 ± 0.0277	0.707 ± 0.00468
CYP2D6	Quinidine	0.971 ± 0.0110	0.964 ± 0.0136	0.967 ± 0.0179	0.864 ± 0.0167	0.789 ± 0.0300	0.593 ± 0.0367
	Paroxetine	0.683 ± 0.152	0.620 ± 0.102	0.423 ± 0.0171	0.211 ± 0.0456	0.0849 ± 0.0111	0.0370 ± 0.00378
CYP3A	Ketoconazole	0.481 ± 0.117	0.391 ± 0.101	0.336 ± 0.0186	0.240 ± 0.0163	0.124 ± 0.0233	0.0593 ± 0.0169
	CYP3cide	0.824 ± 0.0608	0.821 ± 0.0467	0.835 ± 0.0321	0.781 ± 0.0882	0.755 ± 0.0171	0.626 ± 0.00887
	Troleandomycin	1; unbound at all concentrations*					
Pan-CYP	Methoxsalen	0.915 ± 0.0488	0.947 ± 0.00866	0.984 ± 0.0157	0.945 ± 0.0780	1.090 ± 0.0198*	1.100 ± 0.196 *

Values represent the mean and SD for N=3 replicates.

(*) Inhibitors with low affinity for nonspecific binding to microsomal protein as indicated by fu_{mic} values equal to 1. For these inhibitors, nominal and unbound concentrations were considered equivalent.

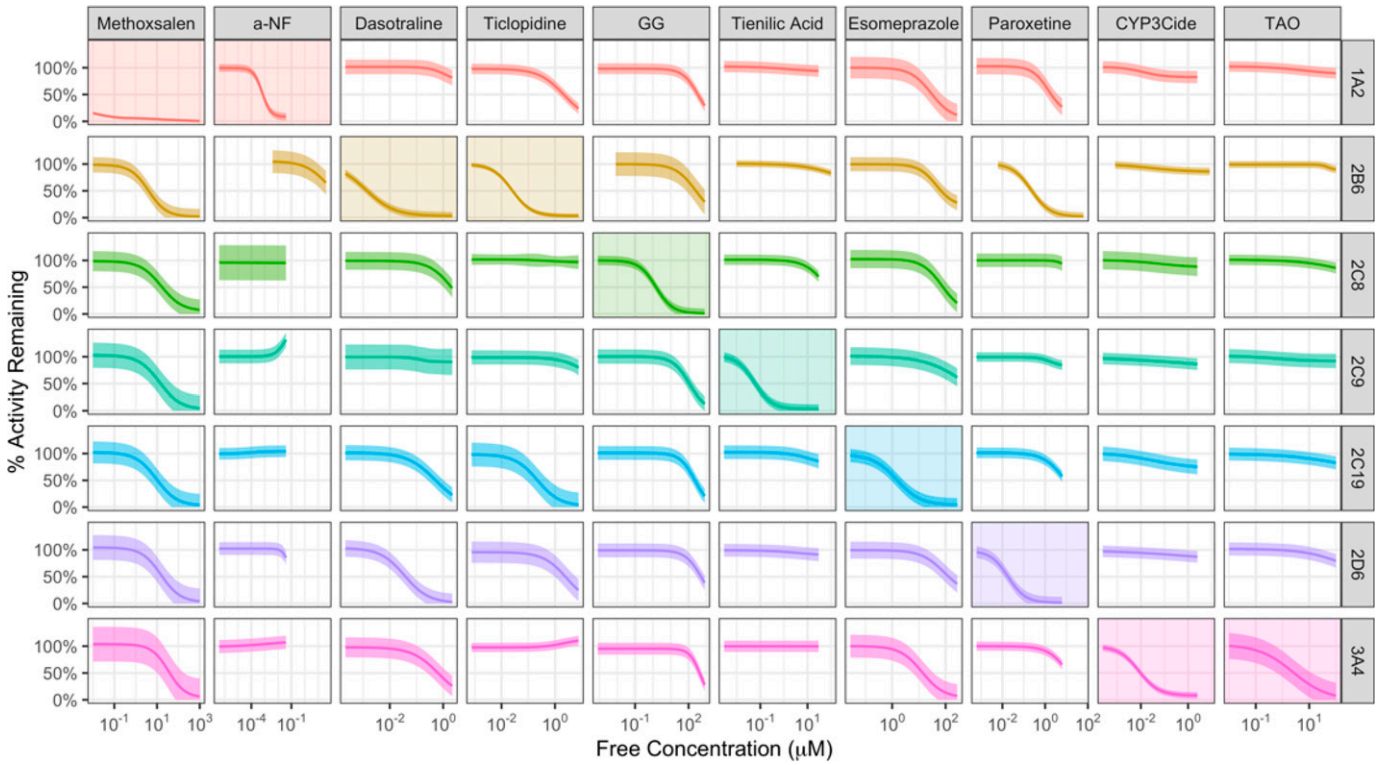

Fig. 3. Inhibition Curves for Alternate Inhibitors. Data represent line of best fit (solid line) and 95% confidence interval (shaded) from $N = 2–3$ experiments. Abbreviations: α-NF, α-naphthoflavone; GG: gemfibrozil glucuronide; TAO: troleandomycin.

($IC_{50,u}$ of 0.728 nM) with good selectivity versus the remaining CYP isoforms. However, stimulation of CYP2C9-mediated diclofenac hydroxylation activity was observed with α-naphthoflavone at concentrations greater than 0.1 μM. Furafylline inhibited CYP1A2 with an $IC_{50,u}$ of 0.139 μM and was selective, demonstrating off-target inhibition only at concentrations greater than 10 μM, resulting in >100-fold selectivity. Furafylline was tested as a TDI of CYP1A2 (Fairman et al., 2007; Racha et al., 1998) following preincubation with HLM; however, it should be considered that selectivity will be even greater with dilution of the inactivation mixture prior to activity measurement with substrate. The potency of methoxsalen for CYP1A2 inhibition under the current experimental conditions was an order of magnitude greater for CYP1A2 ($IC_{50,u}$ < 10 nM) than for other CYP isoforms, of which the next most potent $IC_{50,u}$ was 3.83 μM against CYP2B6. However, under these conditions methoxsalen is expected to inhibit CYP2A6, an isoform not included in our investigations, based on previously reported K_I values ranging from 0.33–1.9 μM (Draper et al., 1997, Koenigs et al., 1998; Kharasch et al., 2000). Significant inhibition (>50%) of the remaining CYP isoforms by methoxsalen concentrations greater than 10 μM was consistent with its utility as a pan-CYP inhibitor as suggested by Palarcharla et al. (2019).

Inhibitors Targeting CYP2B6. The IC_{50} of the TDI 2-phenyl-2-1(1-piperidinyl)propane (PPP) against target isoform CYP2B6 and the next most potently inhibited off-target isoform (CYP2D6) represented ∼54-fold selectivity for CYP2B6. PPP is a TDI of CYP2B6 (Chun et al., 2000; Walsky et al., 2007), and it should be considered that selectivity could be even greater when the pre-incubation mixture is diluted before addition of the substrate. In HLM, dasotraline was a potent inhibitor of CYP2B6 ($IC_{50,u}$ of 1.43 nM); however, selectivity over the next reported isoform, CYP2D6, was only 27-fold. These findings are similar to the inhibitory selectivity of dasotraline reported in human hepatocytes (Yang et al., 2019) and to our knowledge represent the first published report of dasotraline inhibition activity in HLMs. Ticlopidine was a potent inhibitor of CYP2B6 ($IC_{50,u}$ 25.9 nM) with poor selectivity of approximately only ninefold versus CYP2C19 ($IC_{50,u}$ 22.2 nM), and ∼82- to 94-fold versus CYP1A2 and CYP2D6, respectively.

Inhibitors Targeting CYP2C8. Montelukast was a highly potent inhibitor of CYP2C8 with an $IC_{50,u}$ of 93.1 pM. It should be noted that montelukast demonstrates high non-specific binding to microsomes and will exhibit nominal IC_{50} values that are dependent on the microsomal concentration employed. It was 77-fold selective, with CYP2C9 as the next most potently inhibited enzyme. Gemfibrozil glucuronide was also evaluated and showed 74-fold selectivity versus CYP2C9; however, it also showed inhibition against other CYPs. Gemfibrozil glucuronide is a TDI of CYP2C8 (Baer et al., 2009), and selectivity may be even greater when the pre-incubation mixture is diluted before addition of substrate.

Inhibitors Targeting CYP2C9. Sulfaphenazole and tienilic acid were among the most potent and selective of all the inhibitors tested with sulfaphenazole having >500-fold selectivity for CYP2C9 ($IC_{50,u}$ 0.120 μM) versus the next isoform (CYP3A4). Tienilic acid was potent for CYP2C9 ($IC_{50,u}$ 61.1 nM) even without a dilution step to leverage the mechanism-based inhibition property known for this compound.

Inhibitors Targeting CYP2C19. N-Benzylnirvanol was a highly selective inhibitor for CYP2C19 ($IC_{50,u}$ 51.1 nM) with >300-fold selectivity over CYP3A4 and CYP2C8. When used as a reversible inhibitor, esomeprazole demonstrated only 9-fold selectivity for CYP2C19 inhibition versus CYP3A4 as well as noteworthy inhibition of CYP1A2, CYP2B6, CYP2C8, and CYP2D6. However, it should be noted that esomeprazole is reported as a TDI of CYP2C19 (Ogilvie et al., 2011) and that selectivity is likely improved when subject to preincubation with microsomes and NADPH prior to addition of substrate.

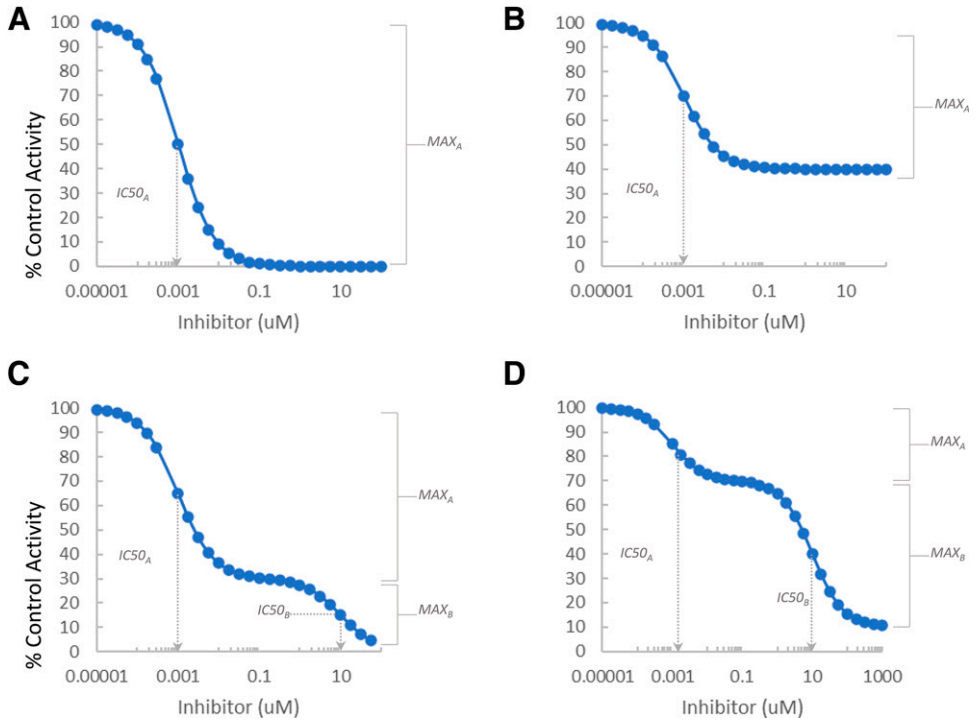

Fig. 4. Theoretical Inhibition Profiles Resulting from 6-Parameter Modeling. Profiles demonstrating inhibitor activity effecting a single target enzyme contributing 100% of reaction activity with IC_{50A} (A), complete inhibition of a single target enzyme contributing 60% of reaction activity with IC_{50A} (B), complete inhibition of target enzyme contributing 70% of reaction activity by inhibitor with IC_{50A} for target isoform and IC_{50B} for off-target isoform (C), inhibition of target enzyme contributing 30% of reaction activity by inhibitor with IC_{50A} for target isoform and IC_{50B} for off-target isoform.

Inhibitors Targeting CYP2D6. Quinidine was a potent and selective inhibitor of CYP2D6 ($IC_{50,u}$ 15.0 nM), with negligible effects (>2000-fold selectivity) on other off-target isoforms. Paroxetine demonstrated similar potency for CYP2D6 but lower selectivity of only 13-fold over the next most potently inhibited enzyme CYP2B6. Paroxetine is a known TDI (Bertelsen et al., 2003), and its true selectivity requires evaluation with a dilution step that follows preincubation. However, when employing a protocol wherein inhibitor and test substrate are co-incubated, quinidine offers a superior choice over paroxetine.

Inhibitors Targeting CYP3A4. The most potent inhibitors of human liver microsomal midazolam 1'-hydroxylase activity were ketoconazole ($IC_{50,u}$ 2.95 nM), CYP3cide ($IC_{50,u}$ 9.72 nM) and troleandomycin ($IC_{50,u}$ 2.71 μM). Surprisingly, off target inhibition of all six of the other isoforms by ketoconazole was significant based on absolute $IC_{50,u}$ values ranging from the most potent, 0.316 μM (CYP2B6) and 0.617 μM (CYP2C8), to 1.80 μM for CYP2D6. In contrast, both CYP3cide and troleandomycin showed little inhibition of other CYP isoform activity within the concentration ranges tested, even when these known TDIs (Walsky et al, 2012; Pessayre et al., 1982) were not subject to a dilution step suggesting improved selectivity profiles relative to ketoconazole. However, using any of these three inhibitors at single concentrations can cause complications (see below).

Desirability Scoring for Inhibitor Comparisons and Optimized Test Concentrations. CYP reaction phenotyping experiments are frequently conducted using single concentrations of inhibitors, for reasons of simplicity and sparing resources. However, as described above, many of the inhibitors employed for this purpose lack enough selectivity to avoid inhibition of off-target CYP enzymes when used at a concentration that effects maximal inhibition of the target CYP. To evaluate this, a desirability score algorithm (Harrington, 1965) was employed to compare the selectivity of the inhibitors and identify optimal single concentrations for use in CYP reaction phenotyping (Table 3). Optimal single concentrations for several of the most selective inhibitors (i.e., α-naphthoflavone, tienilic acid, quinidine, sulfaphenazole, furafylline, and N-benzylnirvanol) were readily identified as achieving >90% inhibition of their respective target CYP enzymes with negligible (<10%) inhibition of any other isoforms (Table 3). For these inhibitors, the reported optimum condition simultaneously achieves maximal inhibition of targeted isoforms with negligible penalties of off-target inhibition.

The inhibitors listed in Table 3 that reside below the solid line lack the selectivity to deliver >90% inhibition of their target enzymes without causing problematic off-target inhibition. Thus, the optimal concentrations for these reflected a compromise of efficacy and selectivity whereby the magnitude of target inhibition was decreased to minimize inhibition of other isoforms. However, even when the target isoform inhibition was less than ideal (<90%) some degree of off-target inhibition was still projected, and it was often the case that one other CYP enzyme was inhibited by at least 10%. If these inhibitors are used at concentrations that yield 95% inhibition of their target enzymes, then substantial off-target inhibition will occur (Table 4). It was noteworthy that a single concentration of the widely used CYP3A4 inhibitor ketoconazole could not be identified that achieves 95% inhibition of CYP3A4 without causing measurable inhibition of several other isoforms. An optimal unbound concentration of 0.030 μM of ketoconazole yields about 88% inhibition of CYP3A while inhibiting CYP2B6 by 14%. However, to achieve 95% inhibition of CYP3A4 with ketoconazole (unbound concentration of 95% inhibition of 0.09 μM), concomitant inhibition of CYP2B6 increased to nearly 30% and that of CYP2C8, CYP2C9, and CYP2C19 all exceed 10%.

Simulated Inhibition Curves from Six-Parameter Curve Fitting. For purposes of illustration, the representative profiles in Fig. 4 were generated to simulate the effects of an inhibitor with 10,000-fold target selectivity on a single enzyme of varying contribution to the overall activity. When off-target inhibition occurs, the 6-parameter model

TABLE 2

Absolute Unbound IC_{50} Values from Inhibitor Selectivity Assessment by Cocktail Assay in Human Liver Microsomes

		Absolute $IC_{50,u}$ (μM)						
Isoform	Inhibitor	1A2	2B6a	2C8	2C9	2C19	2D6	3A4
CYP1A2	Furafylline*	0.139 (0.0863, 0.225)						
	α-Napthoflavone	0.000728 (0.000681, 0.000779)						
CYP2B6	Dasotraline*		0.00143 (0.00125, 0.00164)	2.03 (1.65, 2.51)		0.522 (0.454, 0.6)	0.039 (0.0323, 0.047)	0.638 (0.529, 0.768)
	PPP*		0.742 (0.665, 0.828)				39.9 (35.1, 45.5)	
	Ticlopidine	2.12 (1.89, 2.38)	0.0259 (0.0246, 0.0273)			0.222 (0.156, 0.315)	2.44 (1.95, 3.05)	
CYP2C8	Montelukast		0.0268 (0.0246, 0.0292)	0.0000931 (0.0000806, 0.000108)	0.00714 (0.00617, 0.00827)			
	GG*	335 (298, 376)	259 (179, 374)	1.51 (1.33, 1.71)	112 (95.8, 130)	229 (199, 263)	501 (424, 593)	417 (376, 463)
CYP2C9	Sulfaphenazole				0.120 (0.0946, 0.152)			64.2 (27.4, 150)
	Tienilic Acid*				0.0611 (0.0552, 0.0675)			
CYP2C19	N-Benzylnirvanol			32.6 (11.2, 94.7)		0.0511 (0.0371, 0.0703)		18.6 (10.2, 34)
	Esomeprazole*	31.6 (22.4, 44.8)	68.2 (44.4, 105)	80.3 (49.4, 131)		1.55 (1.35, 1.79)	130 (52.1, 326)	14.1 (10.5, 18.9)
CYP2D6	Quinidine						0.0150 (0.0138, 0.0163)	
	Paroxetine*	1.93 (1.08, 3.44)	0.239 (0.214, 0.267)				0.0183 (0.016, 0.0209)	
CYP3A4/5	Ketoconazole		0.316 (0.295, 0.338)	0.617 (0.295, 1.29)	1.31 (1.16, 1.48)	0.859 (0.76, 0.971)	1.80 (1.56, 2.08)	0.00295 (0.00271, 0.0032)
	Troleandomycin*							2.71 (1.93, 3.8)
	CYP3Cide*							0.00972 (0.00894, 0.0106)
Pan-CYP	Methoxsalen*	<0.01	3.83 (3.14, 4.67)	16.4 (11.2, 24.1)	13.9 (9.02, 21.5)	9.87 (6.92, 14.1)	16.7 (11.2, 24.8)	37.0 (21.5, 63.6)

Data represent mean and 95% confidence interval from N=2–3 experiments.
(*) TDIs subjected to 10 min preincubation in HLM (0.03 mg/ml of protein) with NADPH.
∼ Values extrapolated beyond measured data and included for approximation of off-target activity.
[a] Inhibition of CYP2B6 was assessed separately from the cocktail assay.

TABLE 3

Recommended Single-Concentration, Desirability Score, and Selectivity Profiles of Optimum Inhibitor Selectivity Conditions

Data for 16 inhibitors ranked by desirability scoring of individual curve analysis of target- versus most-inhibited off-target inhibition curves. Values in bold-face type represent the inhibition of the target enzyme for each inhibitor. Dashed entries indicate less than 1% inhibition. Selective inhibitors achieving >90% target inhibition with <10% off target activity are positioned above the bold line. An analysis of the optimal target condition for methoxsalen was not conducted given its evaluation within these studies as a pan-CYP inhibitor.

Compound	Target Isoform	Optimal Unbound Concentration (μM)	Desirability Score	% Inhibition						
				1A2	2B6	2C8	2C9	2C19	2D6	3A4
α-Naphthoflavone	CYP1A2	0.02	0.991	**91**	–	5	–	–	4	–
Furafylline*	CYP1A2	5	0.961	**96**	2	–	2	5	4	–
Tienilic Acid*	CYP2C9	3	0.987	4	3	4	**96**	3	5	–
Sulfaphenazole	CYP2C9	5	0.968	–	2	–	**96**	1	–	4
N-Benzylnirvanol	CYP2C19	2	0.906	4	7	6	4	**93**	8	8
Quinidine	CYP2D6	1	0.975	1	1	2	5	4	**96**	4
PPP*	CYP2B6	5	0.781	–	**84**	–	–	2	14	4
Dasotraline*	CYP2B6	0.007	0.688	–	**77**	1	–	1	14	4
Ticlopidine*	CYP2B6	0.07	0.561	6	**75**	–	2	24	7	2
Gemfibrozil glucuronide*	CYP2C8	10	0.802	4	8	**85**	9	3	3	5
Montelukast	CYP2C8	0.0008	0.792	7	–	**88**	14	7	5	7
Esomeprazole*	CYP2C19	5	0.54	12	4	2	5	**74**	5	25
Paroxetine*	CYP2D6	0.06	0.606	–	20	–	–	–	**77**	–
CYP3cide*	CYP3A4	0.2	0.797	16	11	8	10	19	9	**89**
Ketoconazole	CYP3A4	0.03	0.78	–	14	1	5	6	3	**88**
Troleandomycin*	CYP3A4	50	0.768	9	6	11	8	15	15	**88**

(*) TDIs subjected to 10 min preincubation in HLM (0.03 mg/ml of protein) with NADPH.

attempts to quantify inhibition parameters for both on- and off-target inhibition and therefore can dissect the maximal contribution of the target enzyme and eliminate confounding data from off-target inhibition. In panel A, the characteristic profile represents the simplest scenario of a single enzyme-catalyzed reaction, such as for well-established CYP marker reactions. In this case, the nominal and absolute IC_{50} are the same, the maximum inhibition value is 100%, and the data are best fit to a simple 4-parameter model. In panel B, the contribution of the enzyme is partial (60%), and the inhibitor is highly selective; therefore, the lower asymptote is flat at high inhibitor concentrations and reflects the maximum inhibition (MAX_A). When these types of data were fit to the 4-parameter model, the MAX_A was less than 100% and the IC_{50A} represented the inflection point midway between the upper and lower asymptotes and not a concentration that yields 50% nominal inhibition. The situation becomes more complex in Panels C and D with profiles representative of frequently encountered drug metabolism reactions comprised of multiple enzymes catalyzing the same reaction combined with inhibitors of suboptimal selectivity. These data require fitting to the 6-parameter model to delineate the important MAX_A values that reflect f_m. The first phase represents metabolism by the enzyme that is targeted by the inhibitor being employed and the second is metabolism catalyzed by a second enzyme that is an off-target enzyme of the inhibitor. The shape of the % activity versus log[I] curve will depend on the relative contributions of the two enzymes (i.e., MAX_A and MAX_B), the span of the inhibitor potencies for the two enzymes (IC_{50A} versus IC_{50B}), and the range of inhibitor concentrations tested. Clearly, fitting the complex 6-parameter function successfully requires a greater number of datapoints than typically employed and a wide span of test concentrations; in the data reported in this study there were >20 concentrations evaluated in replicates that spanned over five orders of magnitude. Furthermore, successful fitting of data to the 6-parameter model is reliant on the precision of replicates and statistical identification of outlier points.

Demonstration of the Utility of Full Inhibition Curves and Six-Parameter Curve Fitting for Reaction Phenotyping: Example of Rosiglitazone N-demethylase. Contributions of CYP2C8 and CYP3A4 to rosiglitazone *N*-demethylase activity in HLM were evaluated by comparing results from single- versus multiple-inhibitor concentration approaches (Table 5). Inhibition of rosiglitazone *N*-demethylase was 68.0% when using the optimum, single montelukast concentration from

TABLE 4

Recommended IC_{95} and Inhibitory Activity Associated with Maximal Target Inhibition by Selected Inhibitors

Conditions of maximal inhibition are provided for inhibitors requiring conditions beyond recommended optimum guidance (Table 3) to achieve approximately 95% loss of target isoform activity. The increased concentrations required to achieve full target isoform inhibition incur larger off-target penalties leading to artificially increased inhibition values. CYP3cide (not shown) was unable to achieve 95% inhibition during the selectivity evaluation. Values in bold-face type represent the inhibition of the target enzymes for each inhibitor.

Compound	Target Isoform	Absolute Unbound IC_{95} of Target (μM)	% Inhibition						
			1A2	2B6	2C8	2C9	2C19	2D6	3A4
PPP*	CYP2B6	560	48	**95**	–	58	73	91	80
Dasotraline*	CYP2B6	0.2	–	**95**	8	6	27	80	25
Ticlopidine*	CYP2B6	0.7	27	**95**	1	4	75	24	–
Gemfibrozil glucuronide*	CYP2C8	45	13	21	**95**	30	15	9	8
Montelukast	CYP2C8	0.003	9	3	**95**	33	14	7	18
Paroxetine*	CYP2D6	0.4	13	61	–	2	5	**95**	4
Esomeprazole*	CYP2C19	150	82	66	67	31	**95**	53	90
Ketoconazole	CYP3A4	0.09	3	28	12	10	14	7	**95**
Troleandomycin*	CYP3A4	200	11	11	18	8	20	26	**95**

(*) TDIs subjected to 10 min preincubation in HLM (0.03 mg/ml of protein) with NADPH.
Dashed entries indicate less than 1% inhibition.

TABLE 5

Quantitation of Isoform Contribution to Rosiglitazone *N*-demethylase Activity in Human Liver Microsomes from Multiple- Versus Single-Inhibitor Concentration Analysis

When necessary for single concentration approach, values were reported for the tested concentration nearest to the targeted optimal condition (within 20%). IC_{50} equivalence from multiple concentration analysis assessed by TOST equivalence procedure and Welch's unpaired two-sample t- test with unequal variances of inhibited versus solvent control applied to single concentration analysis. Data represent mean and 95% confidence interval of N=3 replicates.

		Multiple Concentration Approach				Single Concentration Approach			
Inhibitor (Target Isoform)	Model	$IC_{50A,u}$	MAX_A (%)	$IC_{50B,u}$	MAX_B (%)	% Inhibition	Optimal Unbound Conc.	% Inhibition	Maximal Unbound Conc.
Ketoconazole (CYP3A)	6-parameter	0.00217 μM (0.00115, 0.00409)	14.3 (9.7, 19.0)	1.12 μM (0.56, 2.03)	85.8 (54.8, 117)	18.3 (12.1, 24.5)	0.035 μM	22.2 (16.5, 27.9)	0.093 μM
Troleandomycin* (CYP3A)	4-parameter	18.4 μM (1.05, 322)	22.1 (5.88, 38.2)	—	—	14.9 (9.5, 20.3)	43 μM	15.9[a] (11.0, 20.8	100 μM[a]
Montelukast (CYP2C8)	6-parameter	0.0468 nM (0.0353, 0.0619)	70.8 (61.2, 80.4)	3.79 nM (1.45, 9.88)	24.0 (17.4, 30.6)	68.0 (64.7,71.3)	0.82 nM	81.1 (77.8, 84.4)	3.1 nM

(*) TDIs subjected to 10 min preincubation in HLM (0.03 mg/ml of protein) with NADPH.
[a] Data are reported from incubations containing 100 μM troleandomycin, the highest concentration tested in these experiments due to solubility limitations, 2-fold lower than the $IC_{95,u}$ concentration projected for maximal inhibition.

Table 3. This increased to 81.1% (+13%) under the maximal-montelukast concentration tested, 0.00312 μM, a difference consistent with the observed magnitude of CYP3A4 off-target (18%) inhibition associated with the unbound concentration of 95% inhibition of montelukast from selectivity experiments (Table 4). However, employing multiple concentrations of montelukast and using a detailed 6-parameter fitting of the multiple concentration inhibition curve yielded a CYP2C8 contribution of 70.8%. The montelukast unbound IC_{50A} value of 0.0468 nM for rosiglitazone *N*-demethylation (Table 5) was validated by the equivalence test comparison with the positive control activity amodiaquine N-deethylase ($IC_{50,u}$ 0.0483 nM; Table 6, Fig. 5B). Visible in the inhibition curve (Fig. 5A) was the off-target inhibition of CYP3A at concentrations of montelukast greater than 0.001 μM. Thus, the estimation of f_m for CYP2C8 in rosiglitazone *N*-demethylation from the multiple concentration data (f_m = 0.71) was sandwiched between the projections from the less efficacious optimum and the less selective maximal conditions for single-inhibitor concentration tests.

The other enzyme that contributes to rosiglitazone *N*-demethylation was shown to be CYP3A and both ketoconazole and troleandomycin were evaluated as inhibitors for comparison (Fig. 5A). CYP3A4 contributions of 18.3% and 22.2% were projected from optimal and maximal single ketoconazole concentration analysis, respectively, and these were greater than the estimate of 14.3% made from a full inhibition curve with 6-parameter fitting. Overestimation by the single concentration conditions likely reflected non-selective inhibition of CYP2C8 by ketoconazole under the single concentration conditions. The necessity of the 6-parameter fit was demonstrated by the downward slope of the inhibition curve at concentrations of ketoconazole > 0.1 μM presumably due to off-target inhibition of CYP2C8 activity, the major contributing enzyme in this pathway (Fig. 5A). Estimation of CYP3A4 contribution by a single optimal concentration of troleandomycin was slightly lower than that from curve fitting of the multiple concentration inhibition profile (14.9% versus 22.1%). A simple 4-parameter curve sufficiently fit the troleandomycin inhibition curve. The 2-fold difference in troleandomycin $IC_{50,u}$ values for rosiglitazone versus positive control (Table 6, Fig. 5B) failed the equivalence test, and this was most likely due to variability from the low response magnitude and not a true difference in selectivity.

Discussion

Accurate estimation of contributions to metabolism by individual CYP enzymes by reaction phenotyping methods is integral to a robust prediction of in vivo drug-drug interactions and interindividual variability in pharmacokinetics due to genetic polymorphisms of drug metabolizing enzymes. Although multiple reaction phenotyping tools have been developed over the past decades, isoform-selective chemical inhibition methods are most commonly used and recommended by drug regulatory authorities in combination with a parallel approach, such as recombinant human CYP enzymes. The utility of chemical inhibitors is highly dependent on their selectivity for a target isoform. Successful use

TABLE 6

Statistical Equivalence Testing of IC_{50} Determinations From Rosiglitazone Inhibition Experiments

Comparison of intraexperimental inhibitor potency parameters was conducted by TOST equivalence procedure for verification of inhibitor selectivity. IC_{50} Data represent mean and 95% confidence interval of N=3 replicates.

	IC_{50}		Fold Difference in IC_{50}s (Test/Probe) with 90% Confidence Interval	Significantly 5-Fold Equivalent
Inhibitor (Target Isoform)	Test	Probe Substrate		
Ketoconazole	0.00217 μM[a] (0.00115 to 0.00409)	0.00278 μM[b] (0.00260 to 0.00298)	0.780 (0.457, 1.33)	Y
Troleandomycin*	18.4 μM[a] (1.05 to 322)	9.31 μM[b] (7.47 to 11.6)	1.98 (0.180, 21.7)	N
Montelukast	0.0468 nM[a] (0.0353 to 0.0619)	0.0483 nM[c] (0.0438, 0.0533)	0.968 (0.7550, 1.240)	Y

(*) TDI subjected to 10 min of preincubation in HLM (0.1 mg/ml of protein for rosiglitazone experiment or 0.03 mg/ml of protein for probe substrate experiment) with NADPH.
[a] Referring to inhibition of rosiglitazone N-demethylase activity.
[b] Referring to inhibition of midazolam 1'-hydroxylase activity.
[c] Referring to inhibition of amodiaquine N-demethylase activity.

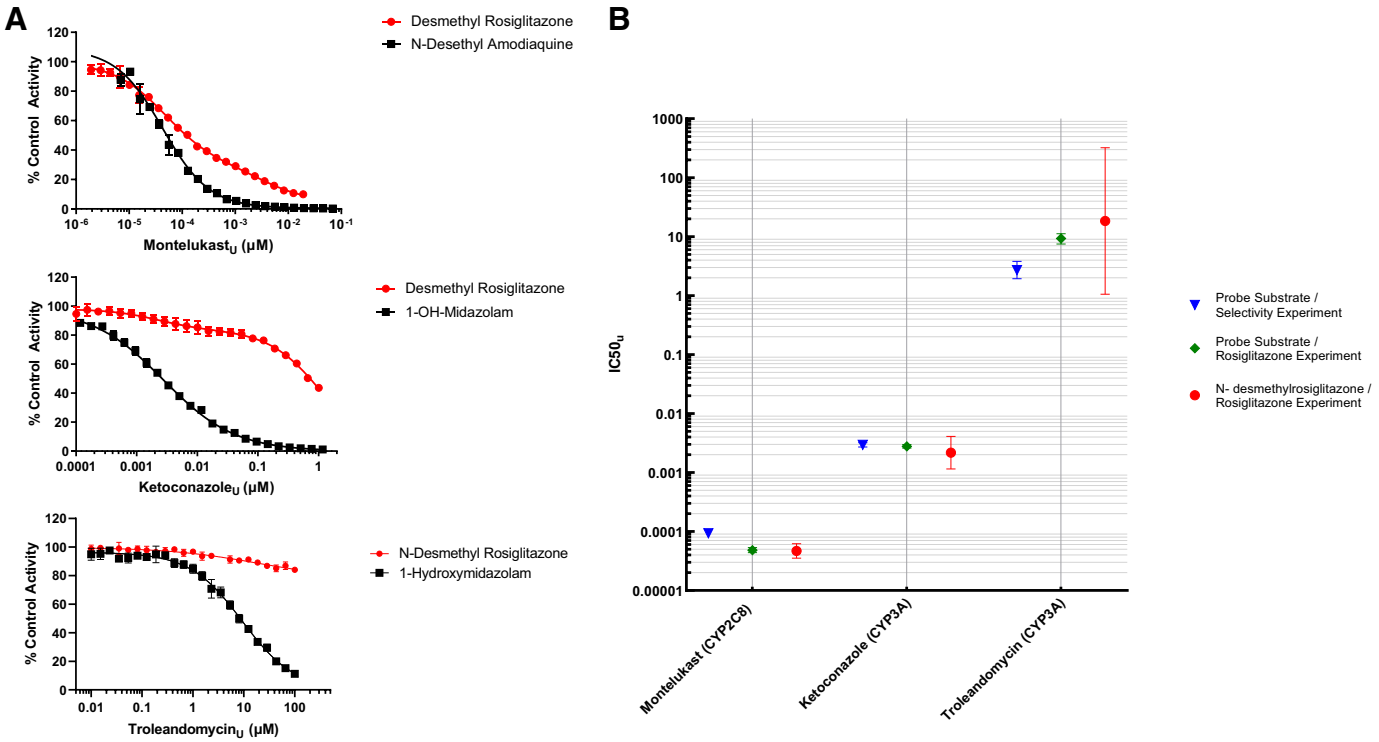

Fig. 5. (A) Rosiglitazone *N*-demethylation in Human Liver Microsomes: Inhibition by Montelukast, Ketoconazole, and Troleandomycin. Inhibition of CYP3A and CYP2C8 activity to rosiglitazone N-demethylation (red circles) and probe substrate reaction (black squares) in HLM by inhibitors montelukast (top panel), ketoconazole (middle panel), and troleandomycin (bottom panel). Nonlinear regression analysis of montelukast and ketoconazole inhibition of *N*-desmethylrosiglitazone formation represent best fit from 6 parameter model. Data points represent mean and SD ($N = 3$). (B) Comparison of intra- and inter- experimental IC_{50} values from montelukast, ketoconazole, and troleandomycin inhibition of rosiglitazone *N*-demethylation and probe substrates.

of an inhibitor requires knowledge of both its broad ranging selectivity among isoforms and the quantitative potency of those interactions.

In the present study, the selectivity of several CYP inhibitors was evaluated, and results were analyzed using a desirability scoring statistical approach (Derringer and Suich, 1980) to provide an optimal, single-concentration recommendation for use during reaction phenotyping. The resulting conditions targeted optimum >90% inhibition of the targeted enzyme while affording <10% inhibition of the next most potently inhibited enzyme (Table 3). The results indicated significant spillover of inhibition to non-targeted CYP isoforms for most of the inhibitors tested. However, the selectivity of some inhibitors was good enough for use as reliable tools for reaction phenotyping. Among the more selective inhibitors were α-naphthoflavone and furafylline for CYP1A2, sulfaphenazole and tienilic acid for CYP2C9, *N*-benzylnirvanol for CYP2C19, and quinidine for CYP2D6. Even under the suggested conditions, these inhibitors are not entirely devoid of off-target effects but rather achieve a delicate balance; true selectivity would require a ≥1000-fold spread in target and off-target enzymes.

For the remaining inhibitors, the optimal concentration yielded insufficient inhibition of the target isoform before simultaneously incurring off target enzyme inhibition greater than 10%. Conditions under which these less selective inhibitors could achieve maximal target inhibition were also considered; however, using the IC_{95} resulted in marked inhibition of multiple off-target CYP enzymes (Table 4). Notable among this group of inhibitors is the presence of the widely used CYP3A inhibitor, ketoconazole. As described above, the optimum ketoconazole condition identified, 0.03 μM, unbound, yielded only 88% inhibition of CYP3A4, while concurrently inhibiting CYP2B6 by 14%. The use of ketoconazole is reportedly further complicated by specific and non-specific binding and stoichiometry relative to the amount of CYP3A4 enzyme in incubations (Tran et al., 2002). The other CYP3A inhibitors tested, troleandomycin and CYP3cide, demonstrated similar selectivity profiles as ketoconazole thereby leaving few options for accurately testing CYP3A4 using a single concentration condition (i.e., typical reported ketoconazole test concentration of 1 μM total), especially concerning given CYP3A is a major contributing DME to many marketed drugs, accounting for up to two thirds of the reported DDIs among drugs approved between 2013–2016 (Yu et al., 2018). For this cohort of inhibitors, the result of discounted off target activity could lead to overestimation of isoform contribution and ultimately to unnecessary conduct of costly victim DDI studies. Although not evaluated in these studies, the inclusion of a dilution step following preincubation would enhance the selectivity of inactivators tested.

To address these shortcomings, it was hypothesized that a more comprehensive study design would improve estimations of f_m values by addressing the often-discounted selectivity problems of single concentration inhibitor usage that leads to cumulative inhibition exceeding 100% across a panel of inhibitors. When generating full inhibition curves with dense datasets over a wide concentration range, it was possible to distinguish between the inhibitor activity toward target and off-target isoforms (of sufficiently separated potency values) using a complex 6-parameter data fitting model. When off-target inhibition occurs, the 6-parameter model quantifies parameters for both on- and off-target inhibition and therefore can dissect the maximal contribution of the target (MAX_A) to eliminate confounding off-target inhibition.

To experimentally demonstrate the approach, rosiglitazone *N*-demethylation was selected as a model drug metabolism reaction since it is known to be catalyzed by multiple CYP enzymes (Bazargan et al., 2017; Baldwin et al., 1999; Park et al., 2004). Montelukast and ketoconazole were employed as typical inhibitors of CYP2C8 and CYP3A4,

and troleandomycin was also evaluated for comparison with the ketoconazole data. CYP2C8 was the largest contributing isoform to the reaction as shown by montelukast inhibition in HLM (Fig. 5A). Visual assessment of the multiphasic concentration response profile was consistent with the selectivity of montelukast (Table 2) and indicative of off-target inhibition at the higher concentrations. This was also evident when comparing the rosiglitazone inhibition data to the inhibition for the CYP2C8 selective marker activity amodiaquine *N*-deethylase, which yields a complete inhibition curve. Statistical analysis confirmed a best-fit of the data with the 6-parameter model in which it was calculated that CYP2C8 contributes 71% of this reaction in HLM (Table 5). Confirmation of the assignment to CYP2C8 was made through demonstration of the statistical equivalence of the observed montelukast IC_{50} for rosiglitazone *N*-demethylation to that of the within-experiment positive control amodiaquine *N*-deethylase reaction (Table 6 and Fig. 5B). The integration of a microsomal binding correction for unbound inhibitor concentration is critical to conducting the statistical determination of equivalence. The inhibition of rosiglitazone formation by montelukast at unbound concentrations greater than 0.001 μM (Fig. 2) resulted in an estimated off-target IC_{50B} value within the range of montelukast off target IC_{50} values for CYP3A4 and CYP2C9 (Table 3) from selectivity studies. These secondary parameters can sometimes provide clues as to the identity of other contributing isoforms, but themselves are not definitive enough for quantitation; use of the inhibitors that target these other enzymes is necessary. A smaller contribution by CYP3A4 to rosiglitazone *N*-demethylation formation was determined from the ketoconazole inhibition profile, which was consistent with multiple phases and best fit to the 6-parameter model. The initial shallow plateau was consistent with a small but significant CYP3A4 contribution of 14% (Fig. 5A; Table 5) and the second phase of inhibition at high inhibitor concentrations was likely spillover to CYP2C8. In contrast, the troleandomycin inhibition profile readily fit to the simpler 4-parameter model due to its improved selectivity versus ketoconazole. It should be noted that the IC_{50} values for troleandomycin inhibition of midazolam 1'-hydroxylase activity in Table 3 and Table 5 differed by 2.7X, and this exemplifies inter-experimental variability that shows the necessity of the use of a positive control marker substrate activity within each experiment and not merely making comparisons to previously obtained data.

From these findings, recommendations on the use of chemical inhibitors for quantitative reaction phenotyping are summarized (Table 7). First, the data clearly show that most CYP inhibitors used in reaction phenotyping have selectivity profiles which may impact the quality of prediction when unaccounted under commonly used single-concentration conditions. Limiting inhibitor concentrations to the optimal condition described will minimize confounding effects due to selectivity. Second, inhibitor evaluations conducted across a wide concentration range and combined with modeling and statistical analysis of the full inhibition curves offers a superior approach to the use of chemical inhibitors in CYP reaction phenotyping, as compared with the more typically used single concentration data. Finally, it must be appreciated that chemical inhibitor studies are one component of a larger phenotyping evaluation. The study designs should be fit-for-purpose with more complex resource-intensive full inhibition curves considered appropriate to influence decision making on clinical pharmacology studies for advanced

TABLE 7

Summary of Recommended Inhibitor Conditions for Use in Reaction Phenotyping Experiments

Recommended conditions for both single and multiple concentration use of chemical inhibitors based on desirability scoring of inhibitor selectivity analysis. The recommended conditions are reported as unbound concentrations along with nominal concentration associated with a 0.1 mg/ml protein condition. Nominal inhibitor concentrations for alternate incubation conditions should be derived by scaling of the recommended unbound concentration by the appropriate microsomal unbound fractions listed in Table 1.

		Optimal Single Concentration (μM) Condition for Inhibition of Target Isoform[a]				Recommended Concentration Range for Multipoint Inhibition Curves	
Inhibitor	Target Isoform	Unbound	Nominal (0.1 mg/ml pt)	% Inhibition		Unbound	Nominal (0.1 mg/ml pt)
α-Naphthoflavone	CYP1A2	0.02	0.1	91	Suitably selective; stimulation of CYP2C9 activity observed at high concentrations	0.0001 – 0.1	0.0005 – 0.5
Tienilic Acid*	CYP2C9	3	3	96	Suitably selective	0.001 – 10	0.001 – 10
Quinidine	CYP2D6	1	1	96	Suitably selective	0.0001 – 1	0.0001 – 1
Sulfaphenazole	CYP2C9	5	5[b]	96	Suitably selective	0.001 – 10	0.001 – 10[b]
Furafylline*	CYP1A2	5	5[b]	96	Suitably selective	0.001 – 10	0.001 – 10[b]
N-Benzylnirvanol	CYP2C19	2	2	93	Suitably selective	0.001 – 10	0.001 – 10
Gemfibrozil glucuronide*	CYP2C8	10	12	85		0.001 – 100	0.001 – 110
CYP3cide*	CYP3A4	0.2	0.2	89	Unable to achieve complete (>95%) inhibition of CYP3A	0.0001 – 1	0.0001 – 1
Montelukast	CYP2C8	0.0008	0.4	88	High nonspecific binding	0.000001 – 0.01	0.0005 – 5
PPP*	CYP2B6	5	5	84		0.01 – 100	0.01 – 100
Ketoconazole	CYP3A4	0.03	0.1	88		0.0001 – 1	0.0003 – 3
Troleandomycin*	CYP3A4	50	50[b]	88	Solubility limitations preclude testing of concentrations >100 μM	0.01 – 100	0.01 – 100[b]
Dasotraline*	CYP2B6	0.007	0.1	77	Best used as a CYP2A6-selective or pan-CYP inhibitor	0.0001 – 1	0.0002 – 20
Paroxetine*	CYP2D6	0.06	0.1	77	Currently not recommended for use in HLMs	0.001 – 1	0.002 – 2
Ticlopidine*	CYP2CB6	0.07	0.09	75	Currently not recommended for use in HLMs	0.001 – 10	0.001 – 15
Esomeprazole*	CYP2C19	5	5	74	Currently not recommended for use in HLMs	0.01 – 100	0.01 – 100

(*) TDI subjected to 10 min preincubation in HLM (0.1 mg/ml of protein for rosiglitazone experiment or 0.03 mg/mL protein for probe substrate experiment) with NADPH. Expectation of improved selectivity when including a preincubation dilution.

[a] Inhibitors listed below the bold line do not achieve >90% inhibition under the recommended optimal condition.

[b] The nominal and unbound concentrations were reported as equivalent for inhibitors with low affinity for nonspecific binding to microsomal protein, as indicated by fu_{mic} values equal to 1.

development candidates for example, whereas the abbreviated single-inhibitor concentration experimental design may suffice to preliminarily assess enzyme involvement when designing optimal drug candidates. Additionally, an informed selection of chemical inhibitors for reaction phenotyping can be guided by foreknowledge of contributing isoforms provided from supporting assays, such as recombinant CYP. The manner in which chemical inhibition data can be best integrated into CYP reaction phenotyping is described in the accompanying report (Doran et al., manuscript submitted). The integrated understanding of chemical inhibitor selectivity should result in improved experimental design, in vitro inhibitor identification, and ultimately improvements in delineation of CYP contribution to drug metabolism.

Acknowledgments

The authors would like to acknowledge Carolyn Richardson for assistance with selectivity experiments.

Authorship Contributions

Participated in research design: Doran, Burchett, Goosen, Obach.

Conducted experiments: Landers, Gualtieri, Balesano, Obach.

Performed data analysis: Doran, Burchett, Landers, Gualtieri, Balesano, Dantonio, Obach.

Wrote or contributed to the writing of the manuscript: Doran, Burchett, Landers, Gualtieri, Dantonio, Goosen, Obach.

References

Baer BR, DeLisle RK, and Allen A (2009) Benzylic oxidation of gemfibrozil-1-O-beta-glucuronide by P450 2C8 leads to heme alkylation and irreversible inhibition. *Chem Res Toxicol* **22**: 1298–1309.

Baldwin SJ, Clarke SE, and Chenery RJ (1999) Characterization of the cytochrome P450 enzymes involved in the in vitro metabolism of rosiglitazone. *Br J Clin Pharmacol* **48**:424–432.

Bazargan M, Foster DJR, Davey AK, and Muhlhausler BS (2017) Rosiglitazone metabolism in human liver microsomes using a substrate depletion method. *Drugs R D* **17**:189–198.

Bertelsen KM, Venkatakrishnan K, Von Moltke LL, Obach RS, and Greenblatt DJ (2003) Apparent mechanism-based inhibition of human CYP2D6 in vitro by paroxetine: comparison with fluoxetine and quinidine. *Drug Metab Dispos* **31**:289–293.

Bjornsson TD, Callaghan JT, Einolf HJ, Fischer V, Gan L, Grimm S, Kao J, King SP, Miwa G, Ni L et al.; Pharmaceutical Research and Manufacturers of America (PhRMA) Drug Metabolism/Clinical Pharmacology Technical Working Group; FDA Center for Drug Evaluation and Research (CDER) (2003) The conduct of in vitro and in vivo drug-drug interaction studies: a Pharmaceutical Research and Manufacturers of America (PhRMA) perspective. *Drug Metab Dispos* **31**:815–832.

Bohnert T, Patel A, Templeton I, Chen Y, Lu C, Lai G, Leung L, Tse S, Einolf HJ, Wang YH et al.; International Consortium for Innovation and Quality in Pharmaceutical Development (IQ) Victim Drug-Drug Interactions Working Group (2016) Evaluation of a new molecular entity as a victim of Metabolic drug-drug interactions-an industry perspective. *Drug Metab Dispos* **44**:1399–1423.

Cerny MA (2016) Prevalence of Non-Cytochrome P450-Mediated Metabolism in Food and Drug Administration-Approved Oral and Intravenous Drugs: 2006-2015. *Drug Metab Dispos* **44**:1246–1252.

Chun J, Kent UM, Moss RM, Sayre LM, and Hollenberg PF (2000) Mechanism-based inactivation of cytochromes P450 2B1 and P450 2B6 by 2-phenyl-2-(1-piperidinyl)propane. *Drug Metab Dispos* **28**:905–911.

Dantonio AL, Doran AC, and Obach RS (2022) Intersystem extrapolation factors (ISEF) are substrate-dependent for CYP3A4: Impact on cytochrome P450 reaction phenotyping. *Drug Metab Dispos* **50**:249–257 DOI: 10.1124/dmd.121.000758.

Derringer G and Suich R (1980) Simultaneous optimization of several response variables. *J Qual Technol* **12**:214–219.

Draper AJ, Madan A, and Parkinson A (1997) Inhibition of coumarin 7-hydroxylase activity in human liver microsomes. *Arch Biochem Biophys* **341**:47–61.

European Medicines Agency (2012) *Guideline on the investigation of drug interactions.*

Fairman DA, Collins C, and Chapple S (2007) Progress curve analysis of CYP1A2 inhibition: a more informative approach to the assessment of mechanism-based inactivation? *Drug Metab Dispos* **35**:2159–2165.

Harrington EC (1965) The Desirability Function. *Industrial Quality Control* **21**:494–498.

Kharasch ED, Hankins DC, and Taraday JK (2000) Single-dose methoxsalen effects on human cytochrome P-450 2A6 activity. *Drug Metab Dispos* **28**:28–33.

Khojasteh SC, Prabhu S, Kenny JR, Halladay JS, and Lu AYH (2011) Chemical inhibitors of cytochrome P450 isoforms in human liver microsomes: a re-evaluation of P450 isoform selectivity. *Eur J Drug Metab Pharmacokinet* **36**:1–16.

Koenigs LL and Trager WF (1998) Mechanism-based inactivation of P450 2A6 by furanocoumarins. *Biochemistry* **37**:10047–10061.

Lindmark B, Lundahl A, Kanebratt KP, Andersson TB, and Isin EM (2018) Human hepatocytes and cytochrome P450-selective inhibitors predict variability in human drug exposure more accurately than human recombinant P450s. *Br J Pharmacol* **175**:2116–2129.

Lu AYH, Wang RW, and Lin JH (2003) Cytochrome P450 in vitro reaction phenotyping: a re-evaluation of approaches used for P450 isoform identification. *Drug Metab Dispos* **31**:345–350.

Nirogi R, Palacharla RC, Uthukam V, Manoharan A, Srikakolapu SR, Kalaikadhiban I, Boggavarapu RK, Ponnamaneni RK, Ajjala DR, and Bhyrapuneni G (2015) Chemical inhibitors of CYP450 enzymes in liver microsomes: combining selectivity and unbound fractions to guide selection of appropriate concentration in phenotyping assays. *Xenobiotica* **45**:95–106.

Ogilvie BW, Usuki E, Yerino P, and Parkinson A (2008) In Vitro approaches for studying the inhibition of drug-metabolizing enzymes and identifying the drug-metabolizing enzymes responsible for the metabolism of drugs (reaction phenotyping) with emphasis on cytochrome, in *Drug–drug interactions, drugs and the pharmaceutical sciences* (Rodrigues AD, ed) p 450, Informa Healthcare, New York.

Ogilvie BW, Yerino P, Kazmi F, Buckley DB, Rostami-Hodjegan A, Paris BL, Toren P, and Parkinson A (2011) The proton pump inhibitor, omeprazole, but not lansoprazole or pantoprazole, is a metabolism-dependent inhibitor of CYP2C19: implications for coadministration with clopidogrel. *Drug Metab Dispos* **39**:2020–2033.

Palacharla RC, Molgara P, Panthangi HR, Boggavarapu RK, Manoharan AK, Ponnamaneni RK, Ajjala DR, and Nirogi R (2019) Methoxsalen as an in vitro phenotyping tool in comparison with 1-aminobenzotriazole. *Xenobiotica* **49**:169–176.

Park JY, Kim KA, Shin JG, and Lee KY (2004) Effect of ketoconazole on the pharmacokinetics of rosiglitazone in healthy subjects. *Br J Clin Pharmacol* **58**:397–402.

Pessayre D, Larrey D, Vitaux J, Breil P, Belghiti J, and Benhamou JP (1982) Formation of an inactive cytochrome P-450 Fe(II)-metabolite complex after administration of troleandomycin in humans. *Biochem Pharmacol* **31**:1699–1704.

Polsky-Fisher SL, Cao H, Lu P, and Gibson CR (2006) Effect of cytochromes P450 chemical inhibitors and monoclonal antibodies on human liver microsomal esterase activity. *Drug Metab Dispos* **34**:1361–1366.

Racha JK, Rettie AE, and Kunze KL (1998) Mechanism-based inactivation of human cytochrome P450 1A2 by furafylline: detection of a 1:1 adduct to protein and evidence for the formation of a novel imidazomethide intermediate. *Biochemistry* **37**:7407–7419.

Rodrigues AD (1999) Integrated cytochrome P450 reaction phenotyping: attempting to bridge the gap between cDNA-expressed cytochromes P450 and native human liver microsomes. *Biochem Pharmacol* **57**:465–480.

Schuirmann DJ (1987) A comparison of the two one-sided tests procedure and the power approach for assessing the equivalence of average bioavailability. *J Pharmacokinet Biopharm* **15**: 657–680.

Shou M, Lu T, Krausz KW, Sai Y, Yang T, Korzekwa KR, Gonzalez FJ, and Gelboin HV (2000) Use of inhibitory monoclonal antibodies to assess the contribution of cytochromes P450 to human drug metabolism. *Eur J Pharmacol* **394**:199–209.

Siu YA and Lai WG (2017) Impact of probe substrate selection on cytochrome P450 reaction phenotyping using the relative activity factor. *Drug Metab Dispos* **45**:183–189.

Tran TH, Von Moltke LL, Venkatakrishnan K, Granda BW, Gibbs MA, Obach RS, Harmatz JS, and Greenblatt DJ (2002) Microsomal protein concentration modifies the apparent inhibitory potency of CYP3A inhibitors. *Drug Metab Dispos* **30**:1441–1445.

US Federal Drug Administration(2020) *In vitro drug interaction studies-cytochrome P450 enzyme- and transporter-mediated drug interactions. Guidance for industry.* (https://www.fda.gov/media/134582/download).

Walker E and Nowacki AS (2011) Understanding equivalence and noninferiority testing. *J Gen Intern Med* **26**:192–196.

Walsky RL and Obach RS (2004) Validated assays for human cytochrome P450 activities. *Drug Metab Dispos* **32**:647–660.

Walsky RL and Obach RS (2007) A Comparison of 2-Phenyl-2-(1-piperidinyl)propane (PPP), 1,1′,1″-Phosphinothioylidynetrisaziridine (ThioTEPA), Clopidogrel, and Ticlopidine as Selective Inactivators of Human Cytochrome P450 2B6. *Drug Metab Dispos* **35**:2053–2059.

Walsky RL, Obach RS, Hyland R, Kang P, Zhou S, West M, Geoghegan KF, Helal CJ, Walker GS, Goosen TC et al. (2012) Selective mechanism-based inactivation of CYP3A4 by CYP3cide (PF-04981517) and its utility as an in vitro tool for delineating the relative roles of CYP3A4 versus CYP3A5 in the metabolism of drugs. *Drug Metab Dispos* **40**:1686–1697.

Wang S, Tang X, Yang T, Xu J, Zhang J, Liu X, and Liu L (2019) Predicted contributions of cytochrome P450s to drug metabolism in human liver microsomes using relative activity factor were dependent on probes. *Xenobiotica* **49**:161–168.

Welch BL (1947) The generalisation of student's problems when several different population variances are involved. *Biometrika* **34**:28–35.

Wienkers LC and Wynalda MA (2002) Multiple cytochrome P450 enzymes responsible for the oxidative metabolism of the substituted (S)-3-phenylpiperidine, (S,S)-3-[3-(methylsulfonyl)-phenyl]-1-propylpiperidine hydrochloride, in human liver microsomes. *Drug Metab Dispos* **30**:1372–1377.

Yang X, Ryu S, and Di L (2019) Dasotraline as a selective cytochrome 2B6 inhibitor for reaction phenotyping. *Biopharm Drug Dispos* **40**:358–361.

Yu J, Zhou Z, Tay-Sontheimer J, Levy RH, and Ragueneau-Majlessi I (2018) Risk of Clinically Relevant Pharmacokinetic-Based Drug-Drug Interactions with Drugs Approved by the U.S. Food and Drug Administration Between 2013 and 2016. *Drug Metab Dispos* **46**:835–845.

Zhang H, Davis CD, Sinz MW, and Rodrigues AD (2007) Cytochrome P450 reaction-phenotyping: an industrial perspective. *Expert Opin Drug Metab Toxicol* **3**:667–687.

Zientek MA and Youdim K (2015) Reaction phenotyping: advances in the experimental strategies used to characterize the contribution of drug-metabolizing enzymes. *Drug Metab Dispos* **43**:163–181.

Address correspondence to: Angela C. Doran, Pfizer Inc., Eastern Point Road, MS 8220-3574, Groton, CT, 06340. E-mail: angela.c.doran@pfizer.com, (m) 860-514-2152